

See discussions, stats, and author profiles for this publication at: <https://www.researchgate.net/publication/265515758>

DNA assisted self-assembly of PAMAM dendrimers

ARTICLE *in* THE JOURNAL OF PHYSICAL CHEMISTRY B · SEPTEMBER 2014

Impact Factor: 3.3 · DOI: 10.1021/jp504175f · Source: PubMed

CITATIONS

2

READS

91

3 AUTHORS:



Taraknath Mandal

Indian Institute of Science

6 PUBLICATIONS 27 CITATIONS

[SEE PROFILE](#)



Mattaparthi Venkata Satish Kumar

Tezpur University

18 PUBLICATIONS 100 CITATIONS

[SEE PROFILE](#)



Prabal K Maiti

Indian Institute of Science

117 PUBLICATIONS 2,566 CITATIONS

[SEE PROFILE](#)

DNA Assisted Self-Assembly of PAMAM Dendrimers

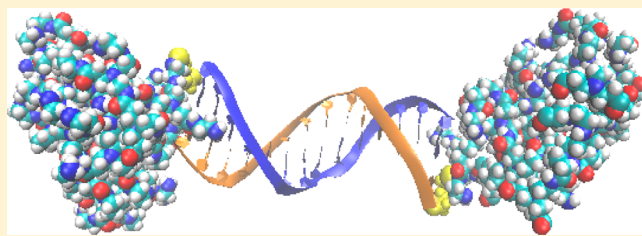
Tarakanath Mandal,[†] Mattaparthi Venkata Satish Kumar,^{†,‡} and Prabal K. Maiti*,[†]

[†]Center for Condensed Matter Theory, Department of Physics, Indian Institute of Science, Bangalore, Karnataka 560 012, India

[‡]Department of Molecular Biology and Biotechnology, Tezpur University, Tezpur, Assam 784 028, India

Supporting Information

ABSTRACT: We report DNA assisted self-assembly of polyamidoamine (PAMAM) dendrimers using all atom Molecular Dynamics (MD) simulations and present a molecular level picture of a DNA-linked PAMAM dendrimer nanocluster, which was first experimentally reported by Choi et al. (*Nano Lett.*, 2004, 4, 391–397). We have used single stranded DNA (ssDNA) to direct the self-assembly process. To explore the effect of pH on this mechanism, we have used both the protonated (low pH) and nonprotonated (high pH) dendrimers. In all cases studied here, we observe that the DNA strand on one dendrimer unit drives self-assembly as it binds to the complementary DNA strand present on the other dendrimer unit, leading to the formation of a DNA-linked dendrimer dimeric complex. However, this binding process strongly depends on the charge of the dendrimer and length of the ssDNA. We observe that the complex with a nonprotonated dendrimer can maintain a DNA length dependent inter-dendrimer distance. In contrast, for complexes with a protonated dendrimer, the inter-dendrimer distance is independent of the DNA length. We attribute this observation to the electrostatic complexation of a negatively charged DNA strand with the positively charged protonated dendrimer.



1. INTRODUCTION

In the field of modern nanotechnology and materials chemistry, there is a great demand for the functional nanomaterials built from specific components with controlled sizes and shapes.^{1,2} For the nanomaterials to have specific applications, well-ordered assembly and blending of nanoscale building objects are considered to be more important. PAMAM dendrimers, which belong to the class of soft nanoparticles, have been considered to be one of the most promising building components to construct nanostructures. This is because of their salient features, such as high functionality, monodisperse nature, control over size, shape, surface valency, and surface functionality in the nanoscale region.³ Among the dendritic families, PAMAM dendrimers were the first to be synthesized, characterized, and commercialized^{4,5} and their derivatives were the most investigated experimentally. They are also shown to have potential applications in drug delivery,^{6–8} diagnostics,⁹ gene transfection,^{10–13} catalysis,¹⁴ and DNA delivery.^{15,16} In the class of PAMAM dendrimer nanoclusters, the building blocks can be coupled through covalent bonds by employing the charge interactions present in them. But this type of linkage of building blocks lands up with complication as specific size ratios and covalent chemistry are highly needed to coordinate the self-assembly. It is also very difficult to assemble various molecules of dendrimers, as they lack specificity. So we thought of an alternative approach that employs the prospects of DNA nanotechnology^{17–24} to assemble PAMAM dendrimers.

In the DNA based self-assembly process, the complex shapes and structures of nanoscale objects are generally held in place through hydrogen bonding of complementary DNA

strands.^{25,26} Some of the recent experiments²⁷ have demonstrated the formation of crystalline structures when DNA links the particles together. There are also some other studies in the literature^{28–33} on the DNA assisted crystallization of colloidal nanoparticles. These results have led to the development of a new generation of DNA-linked materials chemistry. The properties of these DNA-linked crystalline materials are found to depend on various parameters such as DNA length, rigidity of strand, base pair sequence, shape, and size of the nanoparticle.^{32,34–38} There are also several theoretical^{2,25,39–48} and experimental studies^{27,28,30,49–62} on the DNA-based method to assemble the nanoparticles.

Earlier, James Baker's group⁶³ had carried out DNA-directed synthesis of generation five and seven PAMAM dendrimer nanoclusters. Their results suggest that the complementary oligonucleotides can be used to drive the self-assembly of PAMAM dendrimers to form supramolecular nanoclusters. In another study, they have also synthesized dendrimers grafted with various biofunctional materials. Then they used complementary DNA oligonucleotides to link these hybrid structures to form cluster molecules which can be used for targeting cancer cells.⁶⁴ These works have demonstrated the significance of the DNA linked dendrimer nanocluster platform. But to our knowledge, there is no study devoted to the structural and dynamical aspects of the DNA assisted self-assembly of functionalized PAMAM dendrimers at a molecular level. So

Received: April 29, 2014

Revised: September 9, 2014

Published: September 10, 2014



in this current work, we have carried out MD simulations to demonstrate the DNA assisted self-assembly mechanism of PAMAM dendrimers. We have attached DNA strand on one dendrimer molecule to direct the self-assembly by binding to a complementary DNA strand connected to another dendrimer molecule. The schematic representation of the self-assembly process of the PAMAM dendrimers using complementary ssDNAs is shown in Figure 1. To explore the effect of DNA

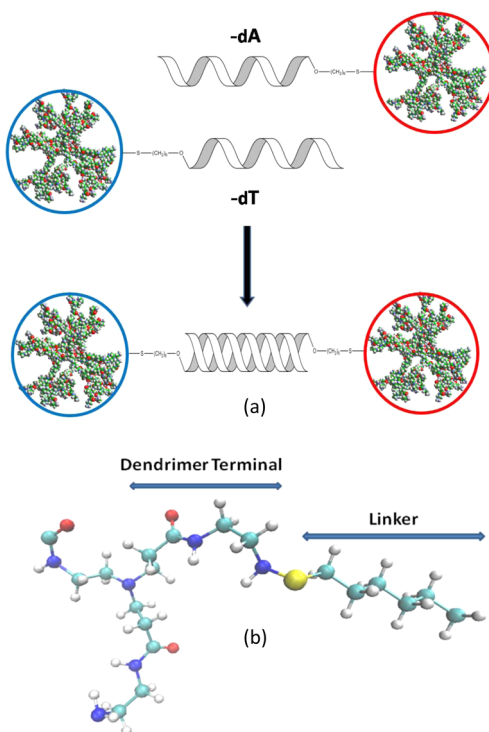


Figure 1. (a) Schematic representation of the self-assembly of G3 PAMAM dendrimers using complementary ssDNA strands. (b) The sulfur atom of the linker molecule is attached to the nitrogen atom of the terminal amine group of the dendrimer. Red, cyan, blue, and white colors represent the oxygen, carbon, nitrogen, and hydrogen atoms, respectively. Sulfur atom is shown in yellow color.

sequence, we have taken ssDNA of adenine (A), thymine (T), guanine (G), and cytosine (C) bases to direct the self-assembly of protonated as well as nonprotonated G3 PAMAM dendrimers.

The rest of the paper is organized as follows: in section 2, we give the details of the building of the initial systems and simulation protocols. We analyze and discuss the results obtained from the simulations in Section 3. And finally, in Section 4, we give a summary of the results.

2. METHODOLOGY

In this work, we have used G3 PAMAM dendrimers as the building blocks to develop DNA-linked dendrimer dimeric complexes. The initial dendrimer structures are generated using our in-house Dendrimer Builder Tool kit (DBT).⁶⁵ The initial structures of the ssDNAs are obtained using nucgen modules of the AMBER package.⁶⁶ To build the initial configurations, we followed the following steps: First, we built the G3-A, G3-T, G3-G, and G3-C subunits separately using the xleap module of AMBER. The first subunit (G3-A) is built by connecting the poly(dA) strand containing adenine bases to the free amino group on the one G3 dendrimer surface via a six carbon alkyl

thiolate [-S(CH₂)₆-] linker. The sulfur atom of the linker molecule is attached to the nitrogen atom of the terminal amine group of the dendrimer as shown in Figure 1(b). The details regarding the construction of the linker molecule can be obtained from our earlier work.⁶⁷ Similarly, the other subunits G3-T, G3-G, and G3-C are built by connecting the poly(dT), poly(dG), and poly(dC) DNA strands to the dendrimer surface, respectively. We then placed two subunits close to each other as shown in Figure 1. The DNA bases of the first subunit are complementary to those of the second subunit. We have followed the similar protocol to build all the dendrimer–ssDNA complexes containing protonated as well as nonprotonated dendrimers as building blocks. The complexes are named as G3-AT-G3 (NP), G3-GC-G3 (NP), G3-AT-G3 (P), and G3-GC-G3 (P). Here -AT- and -GC- represent the complexes containing adenine–thymine and guanine–cytosine complementary bases, respectively whereas NP and P in the parentheses stand for the nonprotonated and protonated dendrimer case, respectively. To explore the effect of ssDNA length on this DNA mediated self-assembly mechanism, we have considered various lengths of ssDNA: 10, 15, 20, and 25 bases of ssDNA for nonprotonated dendrimer case and 10, 15, and 20 ssDNA bases for the protonated dendrimer case. The initially built structures are then solvated using the TIP3P water model⁶⁸ in a way such that at least 15 Å of water shell around the solute exists in all the three directions of the simulation box. The negative charges of the ssDNAs and positive charges of the dendrimer (protonated form) are neutralized by adding appropriate number of Na⁺ and Cl⁻ counterions.

All the MD simulations are performed using the PMEMD module of AMBER software package. PAMAM dendrimers and the linker molecule are described by Generalized Amber Force Field (GAFF),⁶⁹ whereas AMBER03 force field⁷⁰ parameters are used to describe the interactions between the ssDNA atoms. The solvated structures are subjected to 1000 steps of steepest descent minimization of the potential energy, followed by 2000 steps of conjugate gradient minimization. In the minimization step, the entire system excluding the water molecules is kept fixed in their starting conformations using a harmonic constraint with a force constant of 500 kcal/mol/Å². This is done so as to remove the bad contacts between water molecules and the solute. This was followed by another 5000 steps of conjugate gradient minimization while decreasing the force constant of the harmonic restraints from 20 kcal/mol·Å² to zero in steps of 5 kcal/mol·Å². The minimized structures were then subjected to 40 ps of MD using a 2 fs time step for integration. During the MD step, the system was steadily heated from 0 to 300 K using weak 20 kcal/mol·Å² harmonic constraints on the solute to its starting structure. This allows the built in system to undergo slow relaxation. In addition, SHAKE constraints⁷¹ using a geometrical tolerance of 5×10^{-4} Å were imposed on all covalent bonds involving hydrogen atoms. Subsequently, unconstrained MD was performed at constant pressure-constant temperature conditions (NPT), with temperature regulation achieved using the Berendsen weak coupling method⁷² (0.5 ps time constant for heat bath coupling and 0.2 ps pressure relaxation time) to get the correct solvent density. The above-mentioned MD protocol produces very stable MD trajectory for such a complex system which has been demonstrated in our earlier works.^{73–76} Finally, to evaluate the dynamical changes in the system, we have carried out 45–50 ns long NVT MD using a heat bath coupling time constant of 1 ps. The analysis of structural parameters such as

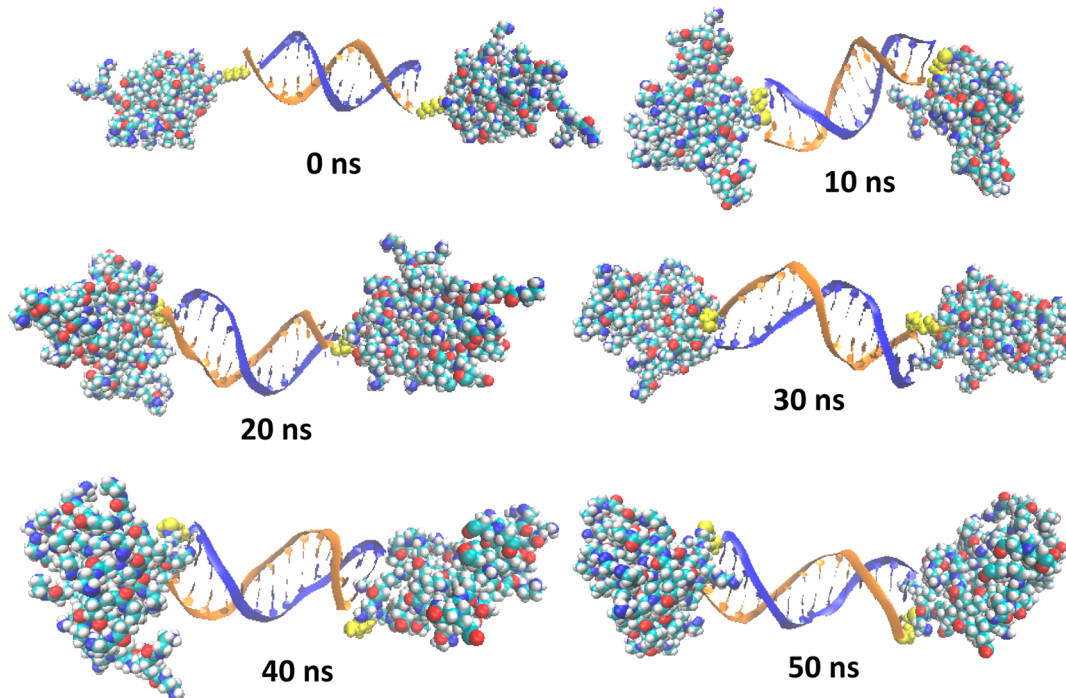


Figure 2. Time evolution of the DNA mediated self-assembled G3 nonprotonated dendrimers using 15 bases long -dA and -dT strands. Blue and orange color represents -dG and -dC strand, respectively. Yellow atoms represent the linker molecule. Note that to ensure shorter self-assembly time, we have placed the ssDNA linked two dendrimer units close by at the beginning of the simulation.

root-mean-square deviation (RMSD), radius of gyration (R_g), and inter-dendrimer distance are carried out using the ptraj module of AMBER package.

3. RESULTS AND DISCUSSION

MD simulations of all the systems performed in this study reveal that ssDNA strand on one dendrimer unit starts a noncovalent, specific base-pair interaction with the complementary DNA strand on the other dendrimer unit to form a dimeric complex. Figure 2 gives the time evolution of the dimeric complex formation with 15 bases long -dG strand attached to one dendrimer hybridizing with the 15 bases long complementary -dC strand attached to another dendrimer. To help accelerate the hybridization kinetics, we have placed the ssDNAs attached to the dendrimer units close to each other. However, we have verified the formation of this dimeric complex with a different initial configuration, where the ssDNAs were kept far apart from each other. In this case also, the ssDNA strands bind with each other to form the complex (see Figure S1 in the Supporting Information, SI). However, the time required for completion of the hybridization process is relatively larger in this case. We have explored the formation of the dimeric complex with different ssDNA lengths and base sequences. Instantaneous snapshots for various dimeric complexes are shown in Figures S2–S9 in the SI. For comparison, we have presented the instantaneous snapshots of the ssDNA (15 bases long) assisted self-assembled complexes for -AT and -GC base sequences in Figure 3. The molecular level pictures of the complexes do not show much dependence on the base sequence. We have also investigated the effect of protonation level of the dendrimer on the complex formation. The molecular level picture of the protonated dendrimer-DNA complex is shown in Figure 4. Even though the complementary DNA strands bind with each other to form

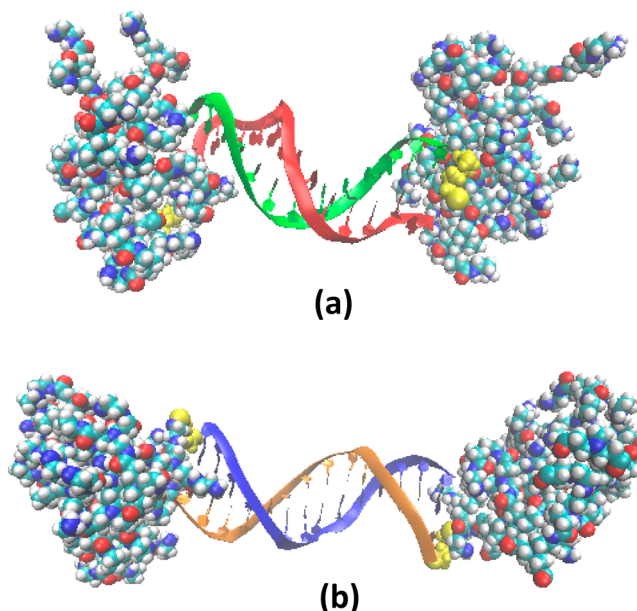


Figure 3. Instantaneous snapshots of the DNA mediated self-assembled G3 nonprotonated dendrimers after 50 ns long MD simulation using (a) -dA and -dT, and (b) -dG and -dC complementary strands of 15 bases long. Red, green, blue, and orange color represents -dA, -dT, -dG, and -dC strands, respectively. Yellow atoms represent the linker molecule.

a dimeric complex in both the protonated and the nonprotonated dendrimer cases, there is a significant difference between the binding mechanisms of these two cases. In the protonated dendrimer cases, the complementary ssDNA strands get attached to each other and at the same time, these hybridized strands wrap the dendrimer surfaces due to electrostatic interactions. In contrast, the hybridized DNA

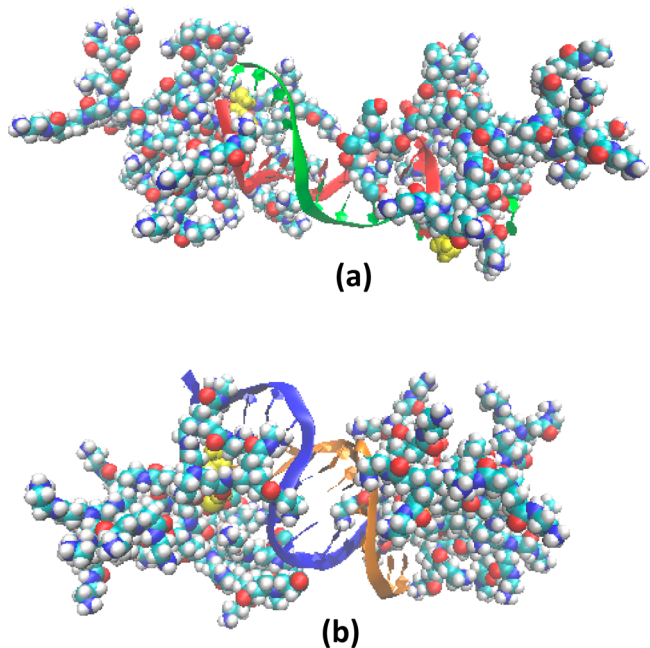


Figure 4. Instantaneous snapshots of the DNA mediated self-assembled G3 protonated dendrimers after 50 ns long MD simulation using (a) -dA and -dT, and (b) -dG and -dC complementary strands of 15 bases long. Red, green, blue and orange color represents -dA, -dT, -dG, and -dC strand, respectively. Yellow atoms represent the linker molecule.

strands do not wrap the nonprotonated dendrimer surfaces. More quantitative analysis will be discussed to probe the extent of wrapping in the subsequent sections. The difference in the binding mechanism is clearly visible from Figures 3 and 4.

We also investigate the conformational changes occurred in different components of the complexes during the time course of MD simulations. First, we concentrate on the linker molecule. Initially, the linker was attached perpendicular to the dendrimer surface. However, after the equilibration of the system, the linker molecule lies flat on the dendrimer surface.

The initial and final configurations of the linker molecule are shown in Figure 5. Thus, the linker molecules do not contribute to the effective size of the complexes. Similar kind of conformational change of the linker molecule are observed for both the protonated and the nonprotonated dendrimer cases studied here. In contrast, the DNA strands interact with the nonprotonated and protonated dendrimers differently. Even though the linker molecule lies flat on the dendrimer surface, the hybridized DNA strands remain perpendicular to the dendrimer surface in case of nonprotonated dendrimers (Figure 3). There is no significant wrapping of the DNA strands on the dendrimer surface. Only one or two bases at the both ends of the DNA penetrate inside the dendrimer. However, in the case of the protonated dendrimer, the complementary DNA strands get attached with each other by base pairing and at the same time, these hybridized strands wrap the surface of both dendrimers (Figure 4). As a result, two protonated dendrimers come closer to each other. To get a quantitative measurement of this wrapping, we have calculated the distance between the ssDNA strand and the host dendrimer corresponding to that strand. This distance is measured by calculating the distance between the center of mass (COM) of the dendrimer and that of the ssDNA attached to that dendrimer. The results for 15 bases long ssDNA are shown in Figure 6. In the case of nonprotonated dendrimer–DNA complex, dendrimer to DNA distances are $34.33 \pm 2.60 \text{ \AA}$ (41), $31.16 \pm 1.57 \text{ \AA}$ (44), $38.62 \pm 3.14 \text{ \AA}$ (47), and $39.59 \pm 2.13 \text{ \AA}$ (44) for -dA, -dT, -dG, and -dC strands, respectively. In contrast, for protonated dendrimer–DNA complexes, dendrimer to DNA distances are $26.08 \pm 1.27 \text{ \AA}$ (48), $19.90 \pm 2.50 \text{ \AA}$ (53), $23.14 \pm 0.97 \text{ \AA}$ (45), and $21.10 \pm 0.86 \text{ \AA}$ (44) for -dA, -dT, -dG, and -dC strand, respectively. The numbers in the parentheses represent the initial values of the dendrimer to DNA distances. Note that the COM distance between the ssDNA and the dendrimer has decreased significantly from its initial value in the protonated dendrimer cases. This large decrease in the ssDNA–dendrimer distance implies that the ssDNA strands are no longer perpendicular to the dendrimer surface, as they were initially at the beginning of the simulation. The ssDNA–dendrimer COM distance does not decrease

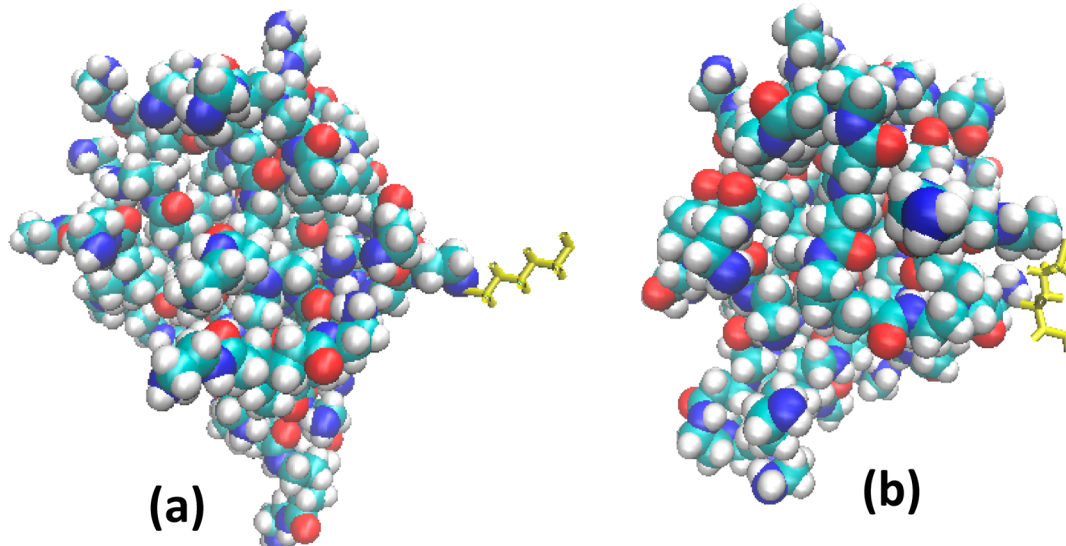


Figure 5. Configuration of the linker molecule (yellow atoms) at the (a) beginning and (b) end of the 50 ns long MD simulation. Note that the linker molecule, which was initially kept perpendicular to the dendrimer surface, lies flat on the dendrimer surface after equilibration.

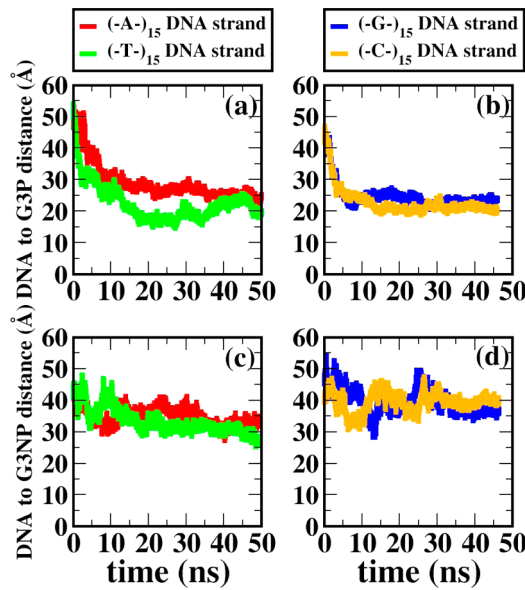


Figure 6. Distance between the dendrimer and ssDNA connected to that dendrimer for (a) G3-AT15-G3-P, (b) G3-GC15-G3-P, (c) G3-AT15-G3-NP, and (d) G3-GC15-G3-NP complexes. P and NP represent the protonated and nonprotonated dendrimers, respectively. The number 15 represents the number of bases of the ssDNAs.

significantly in the case of the nonprotonated dendrimer. The slight decrease from its initial value is due to conformational changes of the linker molecule and the penetration of one or two bases into the dendrimer. This significant adsorption of the ssDNAs on the protonated dendrimer surface is due to the strong electrostatic interaction between the positively charged dendrimer and the negatively charged ssDNAs.⁷³

In Figure 7, we have shown the time evolution of the RMSD of the 15 bases long DNA strands. The initial energy minimized structure is used as a reference structure for the RMSD analysis. The strong binding between the complementary strands leads to the base-pair formation, resulting in very small fluctuations in the RMSD. The RMSD of the DNA strands for both the complexes (containing protonated as well as nonprotonated dendrimers) settle down to a constant value. The RMSD values averaged over last 20 ns of the trajectory are $4.03 \pm 0.30 \text{ \AA}$, $4.06 \pm 0.40 \text{ \AA}$, $3.20 \pm 0.26 \text{ \AA}$, and $5.25 \pm 0.24 \text{ \AA}$ for -dA, -dT, -dG, and -dC strands, respectively, in the protonated dendrimer case. For the nonprotonated dendrimer case, the RMSD values are $3.86 \pm 0.28 \text{ \AA}$, $3.40 \pm 0.39 \text{ \AA}$, $4.00 \pm 0.52 \text{ \AA}$ and $3.10 \pm 0.35 \text{ \AA}$ for -dA, -dT, -dG and -dC strands, respectively (averaged over last 20 ns). In order to get information regarding the degree of compactness and helical properties of the DNA strands, we have calculated various helical parameters of the resulting duplex using Curves program.⁷⁷ The calculated rise and twist of the DNAs for various cases are shown in Figure 8A. We observe that the rise and twist for the protonated dendrimer case fluctuates widely even at the middle region of the DNA strands. These fluctuations indicate the disruption of the base pairing because of the strong interaction of the DNAs with the dendrimers. In contrast for the nonprotonated dendrimer case, both the rise and twist maintain values close to the regular B-DNA values except for few base pairs at both the ends. This is due to the fact that there is not much interaction between the DNA strands and nonprotonated dendrimers. Results of rise and twist calculation suggest that the nonprotonated dendrimer is a better assembling agent for maintaining the regular B-DNA

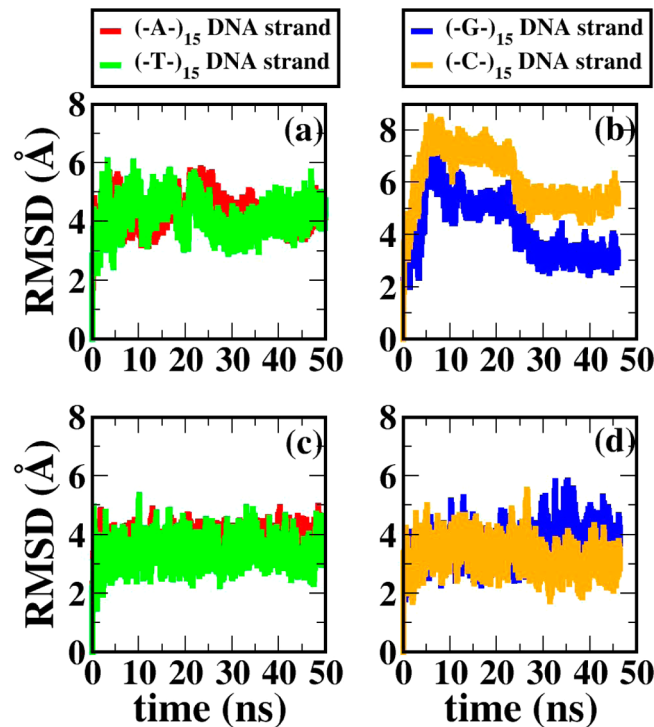


Figure 7. RMSD of the DNA strands of (a) G3-AT15-G3-P, (b) G3-GC15-G3-P, (c) G3-AT15-G3-NP, and (d) G3-GC15-G3-NP complexes. P and NP represent the protonated and nonprotonated dendrimers, respectively. The number 15 represents the number of bases of the ssDNAs.

geometry. Similarly, to check the rigidity of the backbones, we have also calculated the angles between the O3', P, and O5' atoms ($\angle \text{O}3' - \text{P} - \text{O}5'$) of the backbones of the ssDNAs (Figure 8B). Once again, we observe that the fluctuations in the angles exist throughout all the bases and are much larger in the protonated dendrimer cases, compared to the nonprotonated dendrimer cases.

To calculate the effective sizes of the self-assembled structures, we have computed the radius of gyration (R_g) of the whole complex as well as for the individual dendrimers. Figure 9 depicts the time evolution of the R_g of the dendrimer–DNA complex as well as that of individual dendrimer units in the complex for both systems containing protonated and nonprotonated dendrimers. We find that the R_g values of the G3 PAMAM dendrimers are $12.70 \pm 0.22 \text{ \AA}$ and $14.88 \pm 0.15 \text{ \AA}$ in the complex formed by nonprotonated and protonated dendrimers, respectively. These values are in good agreement with the previously^{65,78} reported R_g values for the individual dendrimer, which suggests that there is not much change in the size of the dendrimers compared to the case when they are not linked by DNA. However, we observe that there is a significant decrease in the size of entire complex during the course of MD simulations in the cases where protonated dendrimers are used as the building blocks. This can be attributed to the following reasons: (1) conformational change of the linker molecule which lies flat on the dendrimer surface but initially was kept perpendicular to the dendrimer surface; (2) hybridization between the complementary ssDNAs; and (3) wrapping of the DNA strands on the protonated dendrimer surface. Note that the DNA strand wraps not only the host dendrimer, as it gets hybridized with the complementary ssDNA strand connected to the second dendrimer, it wraps the second dendrimer as

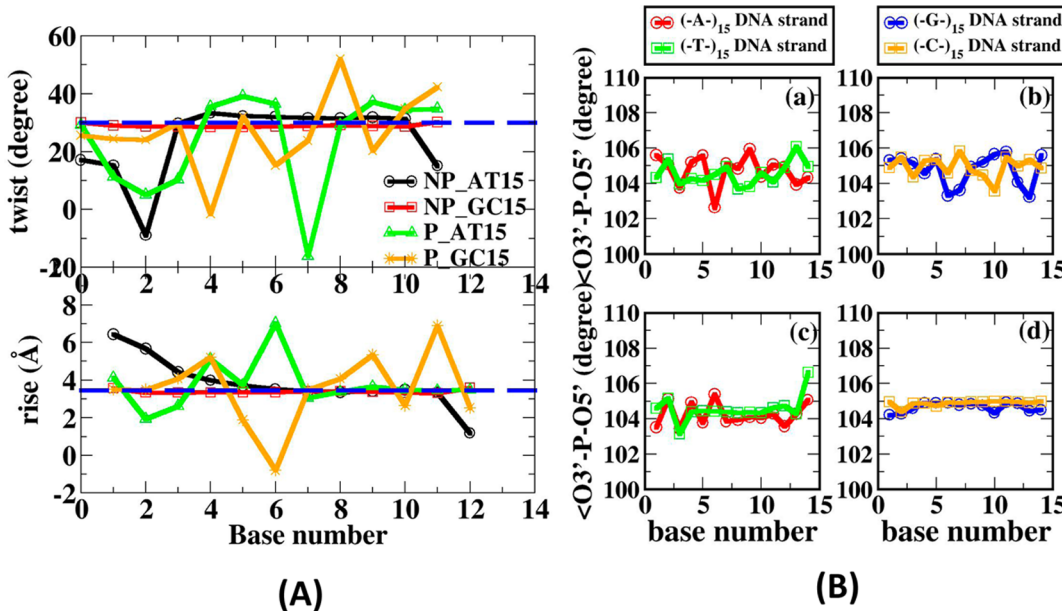


Figure 8. (A) Rise and twist of the DNA base pairs (B) the angles made by O_{3'}, P, and O_{5'} atoms of the backbone for (a) G3-AT15-G3-P (b) G3-GC15-G3-P (c) G3-AT15-G3-NP (d) G3-GC15-G3-NP complexes. P and NP represent the protonated and nonprotonated dendrimers, respectively. The number 15 represents the number of bases of the ssDNAs.

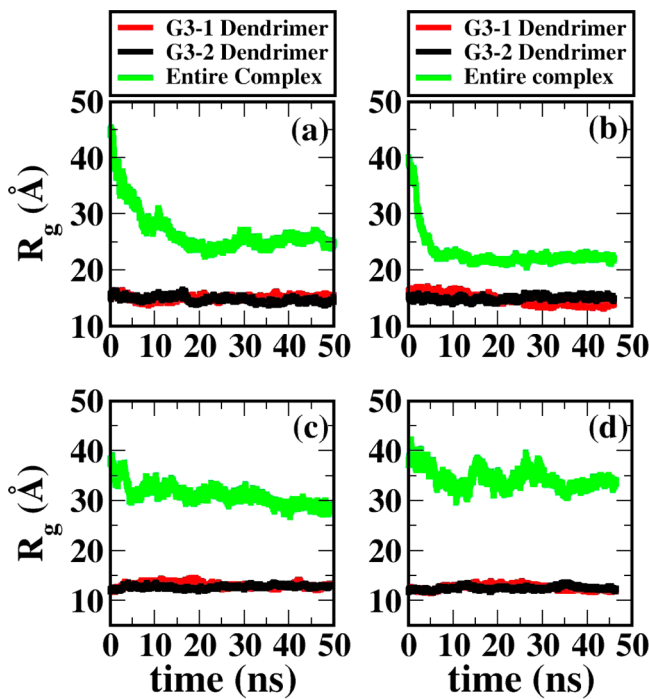


Figure 9. Sizes of the individual dendrimers and the entire complex as a function of time for (a) G3-AT15-G3-P, (b) G3-GC15-G3-P, (c) G3-AT15-G3-NP, and (d) G3-GC15-G3-NP complexes. P and NP represent the protonated and nonprotonated dendrimers, respectively. The number 15 represents the number of bases of the ssDNAs. G3-1 and G3-2 represent the first and second dendrimer, respectively, in the dimeric complex.

well. As a result, both dendrimers come close to each other. And hence, the effective size of the complex decreases significantly from its initial value. However, for the non-protonated dendrimer cases, the effective sizes of the complexes decrease relatively less from its initial value. Slight decrease in the effective size is due to (1) conformational change of the

linker molecule which lies flat on the dendrimer surface, but initially was kept perpendicular to the dendrimer surface and (2) hybridization between the complementary ssDNAs. Because of the lack of wrapping, the size of the complex is not decreased as much as in the case of the protonated dendrimer.

In recent years, self-assembly techniques have been used extensively^{79–82} to decorate the nanoparticles in a desired network. Both the experimental and theoretical studies demonstrated that ssDNAs can be used to control the interparticle distance in a complex network. Here, we have made an attempt to investigate the effect of ssDNA length as well as the effect of different numbers of grafted ssDNA on this self-assembly process. In Figure 10, we have shown the distribution of inter-dendrimer distances for all the systems studied in this work. From the distributions, we observe that the inter-dendrimer distance increases sharply with the ssDNA length in the nonprotonated dendrimer case. In contrast, increase of the inter-dendrimer distance in the protonated dendrimer case is not so prominent. The inter-dendrimer distances for different systems are given in Table 1. We also present the theoretically expected inter-dendrimer distances along with the simulation results (Figure 11). Theoretical calculations are done by considering the average rise per base of the DNA as 3.45 Å and R_g of the G3 nonprotonated dendrimers as ~12.5 Å. In this estimation, we did not consider the length of the linker molecule, as it always lies flat on the dendrimer surface. As we discussed earlier, because of the strong interaction (wrapping) between the DNA strands and protonated dendrimers, the inter-dendrimer distances in these cases are much smaller than the expected values. Thus, the inter-dendrimer distance in the dimeric complex containing protonated dendrimers as building blocks is almost independent of the length of the ssDNA. To study the effect of the salt concentration on the self-assembly process, we have simulated the 15 bases long ssDNA systems at 150 mM NaCl salt concentration. The assembly mechanism is very similar to the

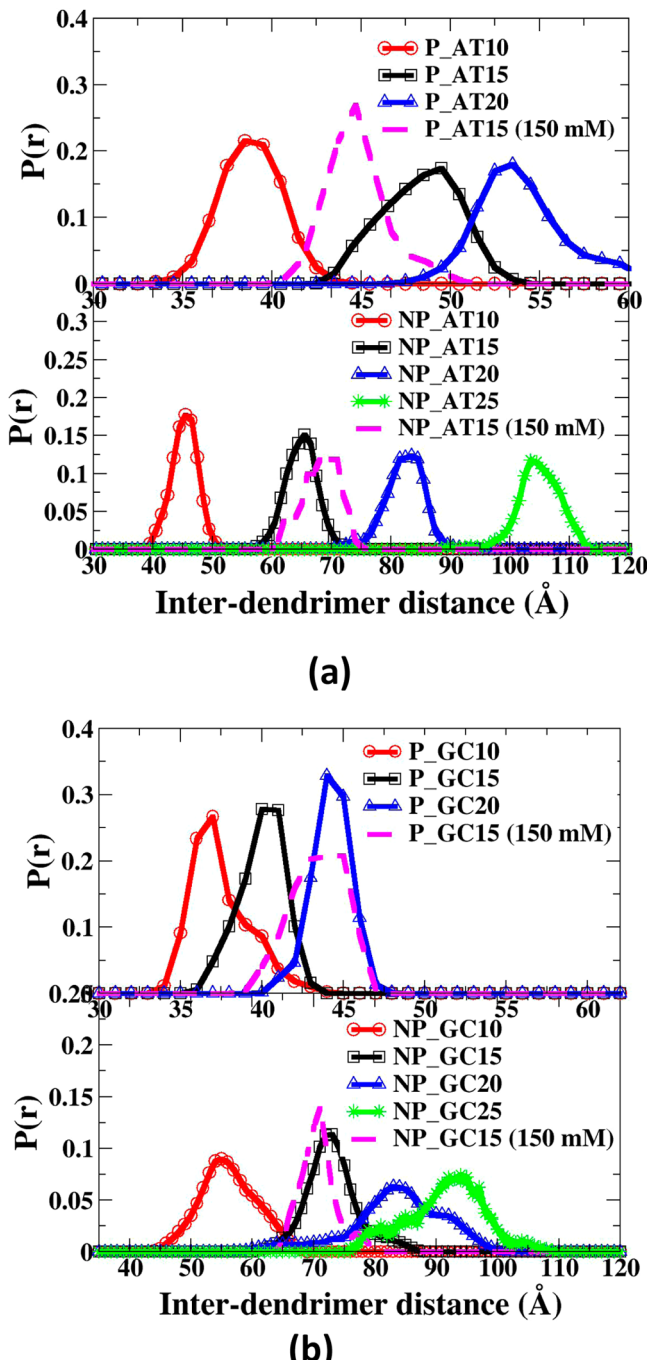


Figure 10. Distribution of the inter-dendrimer distance for different complexes where the assembly is mediated by (a) -AT and (b) -GC DNA sequence, respectively. Upper and lower panels represent the protonated and nonprotonated dendrimer cases, respectively.

case with no extra salt. As shown in Figure 10, similar to the no extra salt cases, the inter-dendrimer distances for the nonprotonated dendrimers are much larger than those of the protonated dendrimer cases. The instantaneous snapshots of the dimeric complex for the 150 mM salt concentration are shown in SI Figures S10 and S11. Thus, we can conclude that the distance between the protonated dendrimers cannot be controlled by changing the length of the grafted ssDNA on the dendrimer surface. However, as expected, the inter-dendrimer distance in the nonprotonated dendrimer cases increases with the length of the ssDNA. We also calculate the rise of DNA

Table 1. Interdendrimer Distance for Different System Investigated in This Study

system	inter-dendrimer distance (Å)
G3NP_AT10	44.7 ± 1.8
G3NP_AT15	64.4 ± 2.5
G3NP_AT15 (150 mM)	67.7 ± 3.0
G3NP_AT20	81.7 ± 3.2
G3NP_AT25	104.3 ± 3.7
G3P_AT10	38.3 ± 1.3
G3P_AT15	47.8 ± 2.0
G3P_AT15 (150 mM)	44.3 ± 1.7
G3P_AT20	53.5 ± 2.5
G3NP_GC10	55.6 ± 4.2
G3NP_GC15	72.5 ± 3.9
G3NP_GC15 (150 mM)	70.2 ± 2.8
G3NP_GC20	83.0 ± 6.6
G3NP_GC25	92.8 ± 6.0
G3P_GC10	37.0 ± 1.8
G3P_GC15	39.5 ± 1.4
G3P_GC15 (150 mM)	42.9 ± 1.6
G3P_GC20	43.7 ± 1.2
G3NP_AT10 (4ssDNA)	52.4 ± 1.8
G3NP_AT10 (3 dendrimer)	49.2 ± 1.5

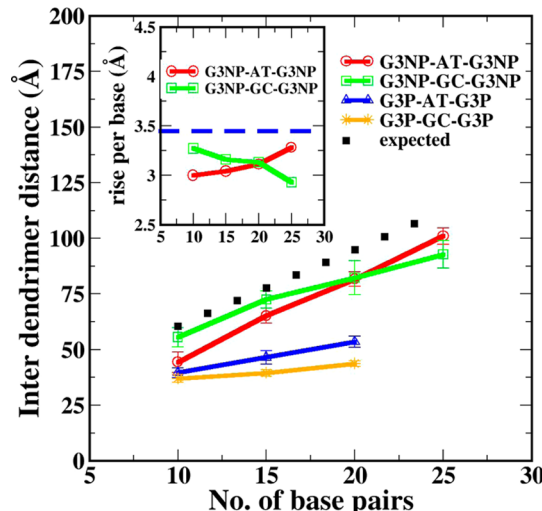


Figure 11. Inter-dendrimer distances as a function of number of DNA base pairs both for the protonated and nonprotonated dendrimer cases. Black dots represent the expected inter-dendrimer distance calculated based on the rise per base pair of 3.45 Å. Rise per base of the hybridized DNAs along the line connecting the dendrimer COM is shown in the inset. Blue dotted lines show the expected values for standard dsDNAs.

base pairs along the line connecting the dendrimer COM for the nonprotonated dendrimer case. The rise of the base pairs is calculated using the following definition: $D = 2R_g + B_s R_b$, where D , R_g , B_s , and R_b are the inter-dendrimer distance, radius of gyration of the dendrimer, number of bases between the two dendrimer surfaces, and rise per base along the line joining the dendrimer COM, respectively. We plot the values of R_b as a function of ssDNA length for both the A-T and G-C complementary strands (inset of Figure 11). We find the average values of R_b to be 3.10 ± 0.12 Å and 3.12 ± 0.14 Å for A-T and G-C pairs, respectively.

Earlier Choi et al.⁶³ reported the synthesis of nanostructures using G7 and G5 PAMAM dendrimers and three sets of

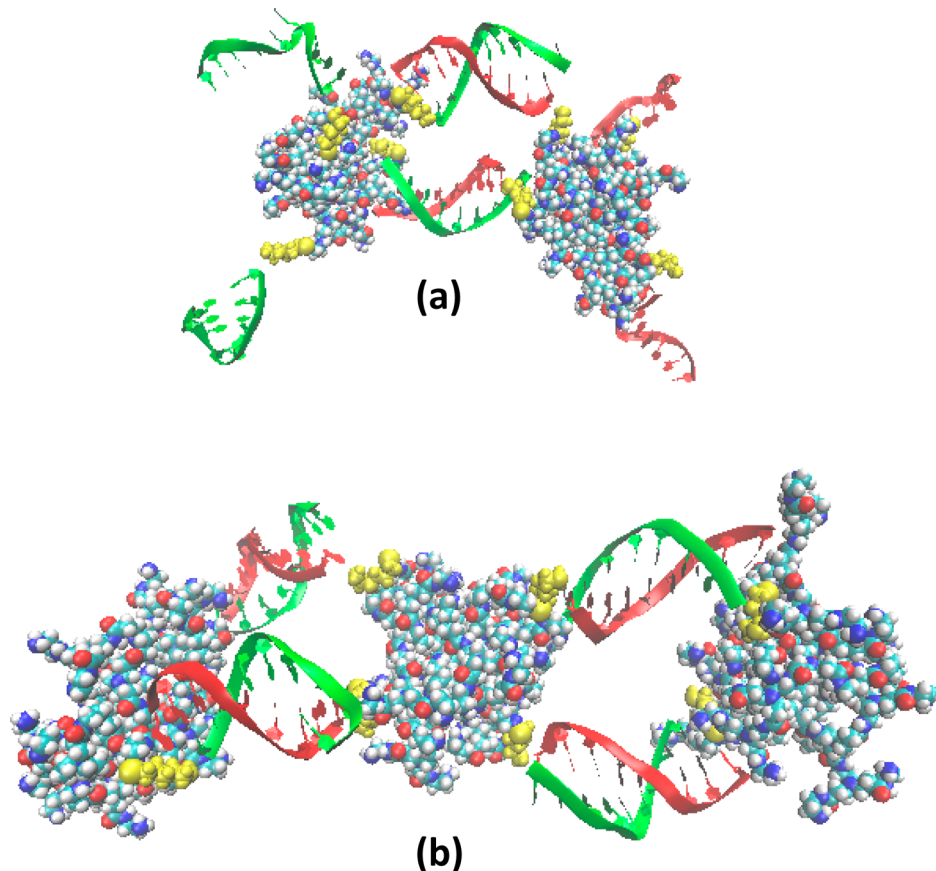


Figure 12. Instantaneous snapshots of the DNA mediated self-assembly of (a) two G3 nonprotonated dendrimers, each connected with four 10 bases long ssDNA of -dA and -dT sequence and (b) three G3 nonprotonated dendrimers, after 50 ns long MD simulation.

complementary oligonucleotides (34, 50, and 66 bases in length). From the AFM image analysis, the inter-dendrimer distance of the nanoclusters linked to the 50-base-long oligonucleotides pairs was found to be 21 ± 2 nm. Authors argued that this distance matches with the theoretical length of the oligonucleotides duplex by using 4.3 Å rise per base for ssDNA. We find little justification as to why a rise of 4.3 Å per base was used when the oligonucleotides were hybridizing and forming duplexes connecting the dendrimer units. However, we notice that during the theoretical estimation, they did not consider the dendrimer size. Thus, considering the R_g of the dendrimers as 5 and 4.7 nm for the G7 and G5 dendrimers, respectively, the average rise per base would be ~ 3.23 Å for a 50 base pairs long dsDNA, which is in good agreement with our observed values (~ 3.11 Å).

So far, we have demonstrated how ssDNA linked to dendrimers can hybridize to form dsDNA linked dimeric complex and how the inter-dendrimer distance can be controlled by changing the length of the ssDNA strands. In all of the previous cases, a single ssDNA is attached to each dendrimer. We have also simulated another variant of the DNA–dendrimer complex where each dendrimer has four ssDNA (10 bases long with an –AT sequence) strands attached to it. The self-assembled DNA–dendrimer complex after 50 ns long dynamics is shown in Figure 12(a). We observe that when the number of attached ssDNA on dendrimer increases, the inter-dendrimer distance increases and is maintained at a value close to theoretically estimated separation as shown in the inter-dendrimer distance distribution in Figure 13. To verify the effectiveness of this method to generate larger scale assembly of

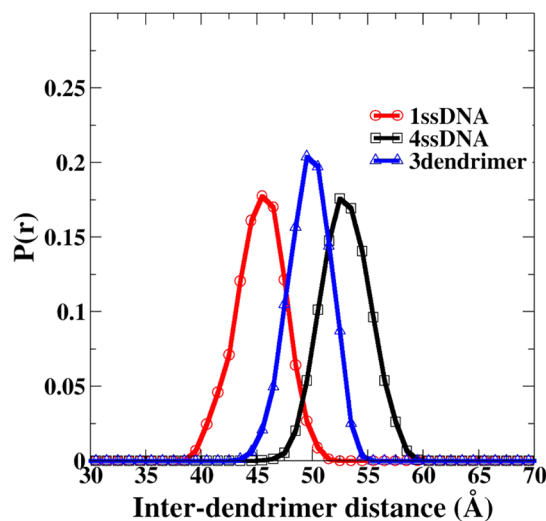


Figure 13. Distribution of inter-dendrimer distance for different complex systems where each dendrimer is linked to one ssDNA (red) and four ssDNA (black). The system containing three dendrimers is shown in blue color. The inter-dendrimer distance is smaller for the dendrimer linked with 1 ssDNA, as compared to the other cases.

DNA–dendrimer complex, we have simulated complex containing many dendrimers with several ssDNA linked to them. For example, in Figure 12(b), we show the instantaneous snapshot of the system having 3 nonprotonated dendrimers. During 50 ns long MD simulation, the dendrimers are assembled at specific inter-dendrimer separation, assisted by

the hybridization of the ssDNA strands. The average inter-dendrimer distance in this case turns out to be 49.2 Å and is comparable to the inter-dendrimer distance (52.4 Å) for the dimeric complex formed by four ssDNA. Thus, this method offers a controllable route to generate larger scale self-assembled structure with well-defined interparticle distance.

4. CONCLUSIONS

Using fully atomistic molecular dynamics simulation, we have demonstrated the DNA mediated self-assembly mechanism of PAMAM dendrimers. We show that the ssDNA attached to the dendrimer surface can direct the self-assembly process by getting hybridized with a complementary ssDNA connected to the second dendrimer surface. To scrutinize the microscopic structures of these dimeric complexes, we have calculated RMSD of the DNAs, R_g of the complexes, and inter-dendrimer distances. From the RMSD analysis, we observe that these complexes are stable, and less fluctuation in RMSD indicates the strong binding between the complementary ssDNAs. Both the R_g and inter-dendrimer distance analysis show that the DNA strands wrap the protonated dendrimer surface. Because of this strong wrapping, the dendrimers come close to each other, making the inter-dendrimer distance almost independent of the ssDNA length. We attribute this wrapping to the electrostatic interaction between the positively charged dendrimer and negatively charged DNAs. However, non-protonated dendrimers can maintain a DNA length dependent inter-dendrimer distance, which increases with the DNA length. We calculate the average rise per base for these hybridized ssDNAs along the line joining the dendrimer centers to be ~3.11 Å. This observation is consistent with some recent studies.⁶³ Thus, our study provides a molecular level picture of the DNA mediated self-assembly of soft nanoparticles.

■ ASSOCIATED CONTENT

S Supporting Information

Instantaneous snapshots of the self-assembly process for various lengths and sequences of ssDNA. This material is available free of charge via the Internet at <http://pubs.acs.org>.

■ AUTHOR INFORMATION

Corresponding Author

*E-mail: maiti@physics.iisc.ernet.in.

Notes

The authors declare no competing financial interest.

■ ACKNOWLEDGMENTS

We thank DST, India for financial assistance. T.M. thanks the Council of Scientific and Industrial Research (CSIR), India for a fellowship.

■ REFERENCES

- (1) Li, H. Y.; LaBean, T. H.; Leong, K. W. Nucleic Acid-Based Nanoengineering: Novel Structures for Biomedical Applications. *Interface Focus* **2011**, *1*, 702–724.
- (2) Storhoff, J. J.; Mirkin, C. A. Programmed Materials Synthesis with DNA. *Chem. Rev.* **1999**, *99*, 1849–1862.
- (3) Esfand, R.; Tomalia, D. A. Poly(Amidoamine) (PAMAM) Dendrimers: From Biomimicry to Drug Delivery and Biomedical Applications. *Drug Discovery Today* **2001**, *6*, 427–436.
- (4) Tomalia, D. A.; Baker, H.; Dewald, J.; Hall, M.; Kallos, G.; Martin, S.; Roeck, J.; Ryder, J.; Smith, P. A New Class of Polymers—Starburst-Dendritic Macromolecules. *Polym. J.* **1985**, *17*, 117–132.
- (5) Tomalia, D. A.; Esfand, R. Dendrons, Dendrimers and Dendrigrafts. *Chem. Ind. (London)* **1997**, 416–420.
- (6) Svenson, S. Dendrimers as Versatile Platform in Drug Delivery Applications. *Eur. J. Pharm. Biopharm.* **2009**, *71*, 445–462.
- (7) Cheng, Y. Y.; Xu, Z. H.; Ma, M. L.; Xu, T. W. Dendrimers as Drug Carriers: Applications in Different Routes of Drug Administration. *J. Pharm. Sci.* **2008**, *97*, 123–143.
- (8) Maingi, V.; Venkata Satish Kumar, M.; Maiti, P. K. PAMAM Dendrimer-Drug Interactions: Effect of pH on the Binding and Release Pattern. *J. Phys. Chem. B* **2012**, *116*, 4370–4376.
- (9) Boas, U.; Heegaard, P. M. H. Dendrimers in Drug Research. *Chem. Soc. Rev.* **2004**, *33*, 43–63.
- (10) Guillot-Nieckowski, M.; Eisler, S.; Diederich, F. Dendritic Vectors for Gene Transfection. *New J. Chem.* **2007**, *31*, 1111–1127.
- (11) Caminade, A. M.; Turrin, C. O.; Majoral, J. P. Dendrimers and DNA: Combinations of Two Special Topologies for Nanomaterials and Biology. *Chem.—Eur. J.* **2008**, *14*, 7422–7432.
- (12) Pavan, G. M.; Posocco, P.; Tagliabue, A.; Maly, M.; Malek, A.; Danani, A.; Ragg, E.; Catapano, C. V.; Prich, S. PAMAM Dendrimers for Sirna Delivery: Computational and Experimental Insights. *Chem.—Eur. J.* **2010**, *16*, 7781–7795.
- (13) Vasumathi, V.; Maiti, P. K. Complexation of Sirna with Dendrimer: A Molecular Modeling Approach. *Macromolecules* **2010**, *43*, 8264–8274.
- (14) Mery, D.; Astruc, D. Dendritic Catalysis: Major Concepts and Recent Progress. *Coord. Chem. Rev.* **2006**, *250*, 1965–1979.
- (15) Nandy, B.; Maiti, P. K. DNA Compaction by a Dendrimer. *J. Phys. Chem. B* **2010**, *115*, 217–230.
- (16) Nandy, B.; Santosh, M.; Maiti, P. K. Interaction of Nucleic Acids with Carbon Nanotubes and Dendrimers. *J. Biosci.* **2012**, *37*, 457–474.
- (17) Seeman, N. C. DNA in a Material World. *Nature* **2003**, *421*, 427–431.
- (18) Seeman, N. C. Nucleic-Acid Junctions and Lattices. *J. Theor. Biol.* **1982**, *99*, 237–247.
- (19) Seeman, N. C. An Overview of Structural DNA Nanotechnology. *Mol. Biotechnol.* **2007**, *37*, 246–257.
- (20) Gothelf, K. V.; LaBean, T. H. DNA-Programmed Assembly of Nanostructures. *Org. Biomol. Chem.* **2005**, *3*, 4023–4037.
- (21) Feldkamp, U.; Niemeyer, C. M. Rational Design of DNA Nanoarchitectures. *Angew. Chem., Int. Ed.* **2006**, *45*, 1856–1876.
- (22) Cai, M. A.; Wang, Q. B. Structural DNA Nanotechnology. *Prog. Chem.* **2010**, *22*, 975–982.
- (23) Aldaye, F. A.; Sleiman, H. F. Supramolecular DNA Nanotechnology. *Pure Appl. Chem.* **2009**, *81*, 2157–2181.
- (24) Jiang, X. H.; Liu, W. Q.; Chen, J. J.; Lin, X. Q. Application of DNA Nanotechnology. *Prog. Chem.* **2007**, *19*, 608–613.
- (25) Aldaye, F. A.; Palmer, A. L.; Sleiman, H. F. Assembling Materials with DNA as the Guide. *Science* **2008**, *321*, 1795–1799.
- (26) Rothemund, P. W. K. Folding DNA to Create Nanoscale Shapes and Patterns. *Nature* **2006**, *440*, 297–302.
- (27) Park, S. Y.; Lee, J. S.; Georganopoulos, D.; Mirkin, C. A.; Schatz, G. C. Structures of DNA-Linked Nanoparticle Aggregates. *J. Phys. Chem. B* **2006**, *110*, 12673–12681.
- (28) Mirkin, C. A.; Letsinger, R. L.; Mucic, R. C.; Storhoff, J. J. A DNA-Based Method for Rationally Assembling Nanoparticles into Macroscopic Materials. *Nature* **1996**, *382*, 607–609.
- (29) Nykypanchuk, D.; Maye, M. M.; van der Lelie, D.; Gang, O. DNA-Guided Crystallization of Colloidal Nanoparticles. *Nature* **2008**, *451*, 549–552.
- (30) Xiong, H. M.; van der Lelie, D.; Gang, O. Phase Behavior of Nanoparticles Assembled by DNA Linkers. *Phys. Rev. Lett.* **2009**, *102*, 015504.
- (31) Sun, D. Z.; Gang, O. Binary Heterogeneous Superlattices Assembled from Quantum Dots and Gold Nanoparticles with DNA. *J. Am. Chem. Soc.* **2011**, *133*, 5252–5254.
- (32) Park, S. Y.; Lytton-Jean, A. K. R.; Lee, B.; Weigand, S.; Schatz, G. C.; Mirkin, C. A. DNA-Programmable Nanoparticle Crystallization. *Nature* **2008**, *451*, 553–556.

- (33) Dai, W.; Kumar, S. K.; Starr, F. W. Universal Two-Step Crystallization of DNA-Functionalized Nanoparticles. *Soft Matter* **2010**, *6*, 6130–6135.
- (34) Macfarlane, R. J.; Lee, B.; Hill, H. D.; Senesi, A. J.; Seifert, S.; Mirkin, C. A. Assembly and Organization Processes in DNA-Directed Colloidal Crystallization. *Proc. Natl. Acad. Sci. U.S.A.* **2009**, *106*, 10493–10498.
- (35) Hurst, S. J.; Hill, H. D.; Mirkin, C. A. “Three-Dimensional Hybridization” With Polyvalent DNA-Gold Nanoparticle Conjugates. *J. Am. Chem. Soc.* **2008**, *130*, 12192–12200.
- (36) Hill, H. D.; Macfarlane, R. J.; Senesi, A. J.; Lee, B.; Park, S. Y.; Mirkin, C. A. Controlling the Lattice Parameters of Gold Nanoparticle Fcc Crystals with Duplex DNA Linkers. *Nano Lett.* **2008**, *8*, 2341–2344.
- (37) Lara, F. V.; Starr, F. W. Stability of DNA-Linked Nanoparticle Crystals I: Effect of Linker Sequence and Length. *Soft Matter* **2011**, *7*, 2085–2093.
- (38) Padovan-Merhar, O.; Lara, F. V.; Starr, F. W. Stability of DNA-Linked Nanoparticle Crystals: Effect of Number of Strands, Core Size, and Rigidity of Strand Attachment. *J. Chem. Phys.* **2011**, *134*, 244701.
- (39) Hsu, C. W.; Sciortino, F.; Starr, F. W. Theoretical Description of a DNA-Linked Nanoparticle Self-Assembly. *Phys. Rev. Lett.* **2010**, *105*, 055502.
- (40) Lee, O. S.; Prytkova, T. R.; Schatz, G. C. Using DNA to Link Gold Nanoparticles, Polymers, and Molecules: A Theoretical Perspective. *J. Phys. Chem. Lett.* **2010**, *1*, 1781–1788.
- (41) Monti, S.; Cacelli, I.; Ferretti, A.; Prampolini, G.; Barone, V. DNA Hybridization Mechanism on Silicon Nanowires: A Molecular Dynamics Approach. *Mol. Biosyst.* **2010**, *6*, 2230–2240.
- (42) Largo, J.; Starr, F. W.; Sciortino, F. Self-Assembling DNA Dendrimers: A Numerical Study. *Langmuir* **2007**, *23*, 5896–5905.
- (43) Knorowski, C.; Travesset, A. Materials Design by DNA Programmed Self-Assembly. *Curr. Opin. Solid State Mater. Sci.* **2011**, *15*, 262–270.
- (44) McLaughlin, C. K.; Hamblin, G. D.; Sleiman, H. F.; Supramolecular, D. N. A. Assembly. *Chem. Soc. Rev.* **2011**, *40*, S647–S656.
- (45) Niemeyer, C. M.; Simon, U. DNA-Based Assembly of Metal Nanoparticles. *Eur. J. Inorg. Chem.* **2005**, *2005*, 3641–3655.
- (46) Dai, W.; Hsu, C. W.; Sciortino, F.; Starr, F. W. Valency Dependence of Polymorphism and Polyamorphism in DNA-Functionalized Nanoparticles. *Langmuir* **2010**, *26*, 3601–3608.
- (47) Di Michele, L.; Varrato, F.; Kotar, J.; Nathan, S. H.; Foffi, G.; Eiser, E., Multistep Kinetic Self-Assembly of DNA-Coated Colloids. *Nat. Commun.* **2013**, *4*.
- (48) Di Michele, L.; Eiser, E. Developments in Understanding and Controlling Self Assembly of DNA-Functionalized Colloids. *Phys. Chem. Chem. Phys.* **2013**, *15*, 3115–3129.
- (49) Smith, B. D.; Liu, J. W. Assembly of DNA-Functionalized Nanoparticles in Alcoholic Solvents Reveals Opposite Thermodynamic and Kinetic Trends for DNA Hybridization. *J. Am. Chem. Soc.* **2010**, *132*, 6300–6301.
- (50) DeMattei, C. R.; Huang, B. H.; Tomalia, D. A. Designed Dendrimer Syntheses by Self-Assembly of Single-Site, SsDNA Functionalized Dendrons. *Nano Lett.* **2004**, *4*, 771–777.
- (51) Puchner, E. M.; Kufer, S. K.; Strackharn, M.; Stahl, S. W.; Gaub, H. E. Nanoparticle Self-Assembly on a DNA-Scaffold Written by Single-Molecule Cut-and-Paste. *Nano Lett.* **2008**, *8*, 3692–3695.
- (52) Mucic, R. C.; Storhoff, J. J.; Mirkin, C. A.; Letsinger, R. L. DNA-Directed Synthesis of Binary Nanoparticle Network Materials. *J. Am. Chem. Soc.* **1998**, *120*, 12674–12675.
- (53) Fan, J. A.; He, Y.; Bao, K.; Wu, C. H.; Bao, J. M.; Schade, N. B.; Manoharan, V. N.; Shvets, G.; Nordlander, P.; Liu, D. R.; Capasso, F. DNA-Enabled Self-Assembly of Plasmonic Nanoclusters. *Nano Lett.* **2011**, *11*, 4859–4864.
- (54) Liu, H. J.; Torring, T.; Dong, M. D.; Rosen, C. B.; Besenbacher, F.; Gothelf, K. V. DNA-Templated Covalent Coupling of G4 PAMAM Dendrimers. *J. Am. Chem. Soc.* **2010**, *132*, 18054–18056.
- (55) Fant, K.; Esbjörner, E. K.; Lincoln, P.; Norden, B. DNA Condensation by PAMAM Dendrimers: Self-Assembly Characteristics and Effect on Transcription. *Biochemistry* **2008**, *47*, 1732–1740.
- (56) Tikhomirov, G.; Hoogland, S.; Lee, P. E.; Fischer, A.; Sargent, E. H.; Kelley, S. O. DNA-Based Programming of Quantum Dot Valency, Self-Assembly and Luminescence. *Nat. Nanotechnol.* **2011**, *6*, 485–490.
- (57) Tang, L. H.; Wang, Y.; Liu, Y.; Li, J. H. DNA-Directed Self-Assembly of Graphene Oxide with Applications to Ultrasensitive Oligonucleotide Assay. *ACS Nano* **2011**, *5*, 3817–3822.
- (58) Gu, H. Z.; Chao, J.; Xiao, S. J.; Seeman, N. C. A Proximity-Based Programmable DNA Nanoscale Assembly Line. *Nature* **2010**, *465*, 202–U86.
- (59) Yao, H.; Yi, C. Q.; Tzang, C. H.; Zhu, J. J.; Yang, M. S. DNA-Directed Self-Assembly of Gold Nanoparticles into Binary and Ternary Nanostructures. *Nanotechnology* **2007**, *18*, 015102.
- (60) Loweth, C. J.; Caldwell, W. B.; Peng, X. G.; Alivisatos, A. P.; Schultz, P. G. DNA-Based Assembly of Gold Nanocrystals. *Angew. Chem., Int. Ed.* **1999**, *38*, 1808–1812.
- (61) Smith, B. D.; Dave, N.; Huang, P. J. J.; Liu, J. W. Assembly of DNA-Functionalized Gold Nanoparticles with Gaps and Overhangs in Linker DNA. *J. Phys. Chem. C* **2011**, *115*, 7851–7857.
- (62) Jahn, S.; Geerts, N.; Eiser, E. DNA-Mediated Two-Dimensional Colloidal Crystallization above Different Attractive Surfaces. *Langmuir* **2010**, *26*, 16921–16927.
- (63) Choi, Y. S.; Mecke, A.; Orr, B. G.; Holl, M. M. B.; Baker, J. R. DNA-Directed Synthesis of Generation 7 and 5 PAMAM Dendrimer Nanoclusters. *Nano Lett.* **2004**, *4*, 391–397.
- (64) Choi, Y.; Thomas, T.; Kotlyar, A.; Islam, M. T.; Baker, J. R. Synthesis and Functional Evaluation of DNA-Assembled Polyamideamine Dendrimer Clusters for Cancer Cell-Specific Targeting. *Chem. Biol.* **2005**, *12*, 35–43.
- (65) Maingi, V.; Jain, V.; Bharatam, P. V.; Maiti, P. K. Dendrimer Building Toolkit: Model Building and Characterization of Various Dendrimer Architectures. *J. Comput. Chem.* **2012**, *33*, 1997–2011.
- (66) Pearlman, D. A.; Case, D. A.; Caldwell, J. W.; Ross, W. S.; Cheatham, T. E.; Debolt, S.; Ferguson, D.; Seibel, G.; Kollman, P. Amber, a Package of Computer-Programs for Applying Molecular Mechanics, Normal-Mode Analysis, Molecular-Dynamics and Free-Energy Calculations to Simulate the Structural and Energetic Properties of Molecules. *Comput. Phys. Commun.* **1995**, *91*, 1–41.
- (67) Venkata Satish Kumar, M.; Maiti, P. K. Structure of DNA-Functionalized Dendrimer Nanoparticles. *Soft Matter* **2012**, *8*, 1893–1900.
- (68) Jorgensen, W. L.; Chandrasekhar, J.; Madura, J. D.; Impey, R. W.; Klein, M. L. Comparison of Simple Potential Functions for Simulating Liquid Water. *J. Chem. Phys.* **1983**, *79*, 926–935.
- (69) Wang, J. M.; Wolf, R. M.; Caldwell, J. W.; Kollman, P. A.; Case, D. A. Development and Testing of a General Amber Force Field. *J. Comput. Chem.* **2004**, *25*, 1157–1174.
- (70) Duan, Y.; Wu, C.; Chowdhury, S.; Lee, M. C.; Xiong, G. M.; Zhang, W.; Yang, R.; Cieplak, P.; Luo, R.; Lee, T. A Point-Charge Force Field for Molecular Mechanics Simulations of Proteins Based on Condensed-Phase Quantum Mechanical Calculations. *J. Comput. Chem.* **2003**, *24*, 1999–2012.
- (71) Ryckaert, J. P.; Cicotti, G.; Berendsen, H. J. C. Numerical-Integration of Cartesian Equations of Motion of a System with Constraints—Molecular-Dynamics of N-Alkanes. *J. Comput. Phys.* **1977**, *23*, 327–341.
- (72) Berendsen, H. J. C.; Postma, J. P. M.; Vangunsteren, W. F.; Dinola, A.; Haak, J. R. Molecular-Dynamics with Coupling to an External Bath. *J. Chem. Phys.* **1984**, *81*, 3684–3690.
- (73) Maiti, P. K.; Bagchi, B. Structure and Dynamics of DNA-Dendrimer Complexation: Role of Counterions, Water, and Base Pair Sequence. *Nano Lett.* **2006**, *6*, 2478–2485.
- (74) Maiti, P. K.; Cagin, T.; Lin, S. T.; Goddard, W. A. Effect of Solvent and pH on the Structure of PAMAM Dendrimers. *Macromolecules* **2005**, *38*, 979–991.

- (75) Maiti, P. K.; Li, Y. Y.; Cagin, T.; Goddard, W. A. Structure of Polyamidoamide Dendrimers up to Limiting Generations: A Mesoscale Description. *J. Chem. Phys.* **2009**, *130*, 144902.
- (76) Maiti, P. K.; Messina, R. Counterion Distribution and Zeta-Potential in PAMAM Dendrimer. *Macromolecules* **2008**, *41*, 5002–5006.
- (77) Lavery, R.; Moakher, M.; Maddocks, J. H.; Petkeviciute, D.; Zakrzewska, K. Conformational Analysis of Nucleic Acids Revisited: Curves. *Nucleic Acids Res.* **2009**, *37*, 5917–5929.
- (78) Maiti, P. K.; Bagchi, B. Diffusion of Flexible, Charged, Nanoscopic Molecules in Solution: Size and pH Dependence for PAMAM Dendrimer. *J. Chem. Phys.* **2009**, *131*, 214901.
- (79) Martinez-Veracoechea, F. J.; Mladek, B. M.; Tkachenko, A. V.; Frenkel, D. Design Rule for Colloidal Crystals of DNA-Functionalized Particles. *Phys. Rev. Lett.* **2011**, *107*, 045902.
- (80) Knorowski, C.; Burleigh, S.; Travasset, A. Dynamics and Statics of DNA-Programmable Nanoparticle Self-Assembly and Crystallization. *Phys. Rev. Lett.* **2011**, *106*, 215501.
- (81) Li, T.; Sknepnek, R.; Macfarlane, R. J.; Mirkin, C. A.; de la Cruz, M. O. Modeling the Crystallization of Spherical Nucleic Acid Nanoparticle Conjugates with Molecular Dynamics Simulations. *Nano Lett.* **2012**, *12*, 2509–2514.
- (82) Mandal, T.; Dasgupta, C.; Maiti, P. K. Engineering Gold Nanoparticle Interaction by PAMAM Dendrimer. *J. Phys. Chem. C* **2013**, *117*, 13627–13636.